# Polymer Chemistry

Accepted Manuscript






ROYAL SOCIETY OF CHEMISTRY

www.rsc.org/polymers

**For Table of Contents use only**

# Dispersion RAFT polymerization: comparison between the monofunctional and bifunctional macromolecular RAFT agents

Chengqiang Gao, Shentong Li, Quanlong Li, Pengfei Shi, Sayyar Ali Shah and Wangqing Zhang*

Key Laboratory of Functional Polymer Materials of the Ministry of Education, Collaborative Innovation Center of Chemical Science and Engineering (Tianjin), Institute of Polymer Chemistry, Nankai University, Tianjin 300071, China.

*To whom correspondence should be addressed. E-mail: wqzhang@nankai.edu.cn, Tel: 86-22-23509794, Fax: 86-22-23503510.

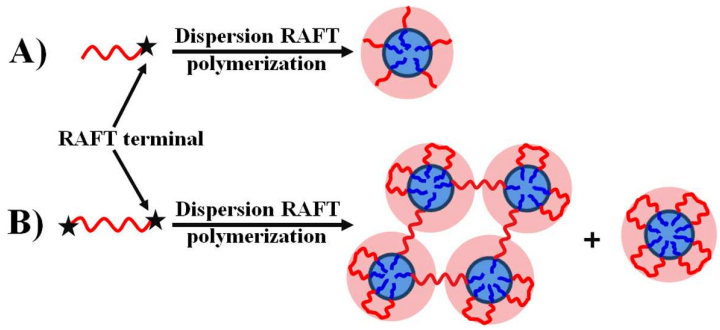


The dispersion RAFT polymerizations mediated with the poly(ethylene glycol) based monofunctional and bifunctional macro-RAFT agents were comparatively studied. These two cases of dispersion RAFT polymerization have similar polymerization kinetics, whereas lead to different block copolymer morphologies.

Cite this: DOI: 10.1039/c0xx00000x

www.rsc.org/xxxxxx

ARTICLE TYPE

# Dispersion RAFT polymerization: comparison between the monofunctional and bifunctional macromolecular RAFT agents

**Chengqiang Gao,[a] Shentong Li,[a] Quanlong Li,[a] Pengfei Shi,[a] Sayyar Ali Shah,[b] and Wangqing Zhang[a]***

***Received (in XXX, XXX) Xth XXXXXXXXX 20XX, Accepted Xth XXXXXXXXX 20XX***

**DOI: 10.1039/b000000x**

**Abstract:** Bifunctional macromolecular RAFT (macro-RAFT) agent mediated polymerization affords one-step synthesis of BAB triblock copolymer, which may has special morphology. However, the bifunctional macro-RAFT agent mediated polymerization under heterogeneous condition is rarely reported. In this contribution, the dispersion RAFT polymerizations of styrene in the methanol/water mixture mediated with the poly(ethylene glycol) based monofunctional and bifunctional macro-RAFT agents, which afford the AB diblock copolymer of poly(ethylene glycol)-*block*-polystyrene (*m*PEG-*b*-PS) and the BAB triblock copolymer of polystyrene-*block*-poly(ethylene glycol)-*block*-polystyrene (PS-*b*-PEG-*b*-PS), respectively, are compared. It is found that these two dispersion RAFT polymerizations have similar polymerization rate, and almost full monomer conversion can be achieved. The molecular weight of both the *m*PEG-*b*-PS diblock copolymer and the PS-*b*-PEG-*b*-PS triblock copolymer linearly increases with the monomer conversion, whereas the control over the polydispersity index (PDI) of the PS-*b*-PEG-*b*-PS triblock copolymer is not as good as that of the *m*PEG-*b*-PS diblock copolymer. The monofunctional macro-RAFT agent mediated dispersion polymerization affords the *in situ* synthesis of the *m*PEG-*b*-PS colloidal nanoparticles, which can be uniformly distributed in the polymerization medium and whose size increases with the extension of the solvophobic PS block. Whereas, the bifunctional macro-RAFT agent mediated dispersion polymerization leads to the mixture of colloidal nanoparticles and gel-like networks of the PS-*b*-PEG-*b*-PS triblock copolymer.

## 1 Introduction

Block copolymer nanoparticles, especially amphiphilic block copolymer nanoparticles, have received great interest for their applications in cosmetics, drug delivery, catalysis, stabilization of emulsions and surface coatings.[1-4] In the past twenty years or so, the self-assembly of amphiphilic block copolymers in the block-selective solvent into block copolymer nano-objects has been widely documented,[5-25] and this strategy is demonstrated to be valid in the preparation of amphiphilic block copolymer nano-objects. For amphiphilic AB diblock copolymers (Note: the A block represents solvophilic block and the B block represents the solvophobic block throughout this manuscript) in the selective solvent for the A block (A-selective solvent), corona-core micelles, in which the A block forms the corona and the B block forms the core, are usually formed.[5-9] The morphology of the ABA triblock copolymer micelles in the A-selective solvent is similar to the AB diblock copolymer micelles in most cases.[10-12] However, the micellization of symmetrical amphiphilic BAB triblock copolymers in the A-selective solvent is much more complex.[13-25] There are three possible BAB triblock copolymer morphologies: (i) flower-like corona-core micelles in which the middle corona-forming A block takes loop conformation with the both-end B blocks located in the same micellar core following the closed association mechanism (Scheme 1A);[13-18] (ii) dangled micelles with one of the insoluble B blocks dangling in the shell (Scheme 1B);[19,20] (iii) branched micellar aggregates including interconnected micelles and gel networks with the two B blocks incorporated in different micellar cores following an open association mechanism (Scheme 1C),[16-25] in the A-selective solvent. The formation of interconnected micelles and gel networks is an important feature which distinguishes BAB triblock copolymers from the AB diblock copolymers.[16-25] This bridging of micelles in addition to entanglement at high concentrations can ultimately lead to BAB triblock copolymer gel.

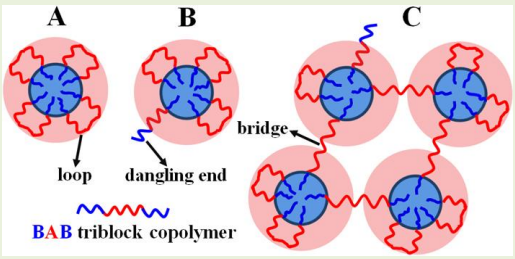


**Scheme 1.** Morphologies of the symmetrical amphiphilic BAB triblock copolymers in the A-selective solvent.

Recently, polymerization-induced self-assembly (PISA) has attracted increasing interest since it offers an efficient route for the *in situ* synthesis of amphiphilic block copolymer nano-objects at relatively high copolymer concentrations (up to 30%),[3,4] which is much beyond the micellization of amphiphilic block copolymers in block-selective solvents. Notable contributions have been made by the research groups led by Charleux,[26,27] Monteiro,[28,29] Cunningham[30] and Hawkett[31,32] in the emulsion RAFT polymerization and by Charleux,[33,34] Pan,[35-37] Armes,[38-40] and An[41-43] in the dispersion RAFT polymerization. We have also found that the character of the macro-RAFT agent including the polymerization degree (DP) of the macro-RAFT agent and the solvophilic/solvophobic balance in the macro-RAFT agent exerts

great influence on the polymerization kinetics and the morphology of the *in situ* synthesized block copolymer nano-objects during the macro-RAFT agent mediated dispersion polymerization.[44-50] Up to the present, the monofunctional macro-RAFT agent has been usually employed either in the emulsion polymerization or in the dispersion polymerization,[26-50] and therefore AB diblock copolymer nano-objects or ABA triblock copolymer nano-objects have been prepared. However, nothing or very little is known about the bifunctional macro-RAFT agent mediated dispersion polymerization and about the morphology of the *in situ* synthesized BAB triblock copolymers under the PISA condition, although this bifunctional macro-RAFT agent mediated polymerization under homogeneous condition has been reported.[20,21,51,52]

In this contribution, the monofunctional macro-RAFT agent of *S*-1-dodecyl-*S*′-(α,α′-dimethyl-α″-acetic acid) trithiocarbonate-terminated poly(ethylene glycol) monomethyl ether (*m*PEG-TTC, in which TTC represents the RAFT terminal of trithiocarbonate) and the bifunctional macro-RAFT agent of bis(*S*-1-dodecyl-*S*′-(α,α′-dimethyl-α″-acetic acid) trithiocarbonate-terminated poly(ethylene glycol) (TTC-PEG-TTC) with similar molecular weight were synthesized (Scheme 2), and their mediated dispersion RAFT polymerizations of styrene and the morphologies of the *in situ* synthesized AB diblock copolymer of poly(ethylene glycol)-*block*-polystyrene (*m*PEG-*b*-PS) and the BAB triblock copolymer of polystyrene-*block*-poly(ethylene glycol)-*block*-polystyrene (PS-*b*-PEG-*b*-PS) are comparatively studied. It is found that, the bifunctional macro-RAFT agent mediated dispersion polymerization of styrene shows a similar polymerization kinetics to that in the presence of the monofunctional macro-RAFT agent, whereas it affords much different block copolymer morphologies. That is, the monofunctional macro-RAFT agent mediated dispersion polymerization leads to AB diblock copolymer colloidal nanoparticles, and the bifunctional macro-RAFT agent mediated dispersion polymerization results in the mixture of BAB triblock copolymer nanoparticles and gel-like networks.

## 2 Experimental

### 2.1 Materials

Styrene (St, >98%, Tianjin Chemical Company, China) was distilled under reduced pressure prior to use. Poly(ethylene glycol) monomethyl ether (*m*$PEG_{113}$-OH, $M_n$ = 5000 g/mol and *m*$PEG_{45}$-OH, $M_n$ = 2000 g/mol, Aldrich) and dihydroxyl-terminated poly(ethylene glycol) (HO-$PEG_{136}$-OH, $M_n$ = 6000 g/mol and HO-$PEG_{45}$-OH, $M_n$ = 2000 g/mol, Alfa Aesar) were purified by azeotropic distillation with dry toluene before use. *S*-1-Dodecyl-*S*′-(α,α′-dimethyl-α″-acetic acid) trithiocarbonate (DDMAT) was synthesized as reported previously.[53] 2,2'-Azobis(isobutyronitrile) (AIBN, >99%, Tianjin Chemical Company, China) was recrystallized from ethanol before being used. Oxalyl chloride [$(COCl)_2$, 98%, Tianjin Chemical Company, China] was freshly distilled before use. Dichloromethane (DCM, >99%, Tianjin Chemical Company, China) was freshly distilled from $CaH_2$ prior to use. All other chemical reagents with analytical grade were purified by standard procedures or used as received. Deionized water was used.

### 2.2 Synthesis of the monofunctional macro-RAFT agent of *m*$PEG_{113}$-TTC and the bifunctional macro-RAFT agent of TTC-$PEG_{136}$-TTC

Into a dry flask, DDMAT (1.46 g, 4.00 mmol) and DCM (20.0 mL) were added, and then dropwise addition of oxalyl chloride [$(COCl)_2$, 1.7 mL, 20.0 mmol] dissolved in DCM (10.0 mL) in 10 min under nitrogen atmosphere was followed. The mixture was magnetically stirred under nitrogen atmosphere at 25 °C for about 2 h until the gas evolution stopped. The solvent and the excess oxalyl chloride were removed by rotary evaporation under vacuum at 30 °C (Note: to remove all the oxalyl chloride, 20 mL of DCM was added to re-dissolve the brown residue and then the rotary evaporation was performed, and the dissolution/evaporation cycles were repeated three times). Into the flask, *m*$PEG_{113}$-OH (10.0 g, 2.00 mmol) or HO-$PEG_{136}$-OH (6.0 g, 1.00 mmol) dissolved in DCM (40.0 mL) was added under nitrogen atmosphere. The reaction was allowed to proceed for 24 h at 25 °C with magnetically stirring under nitrogen atmosphere. The solution was concentrated under reduced pressure, and the polymer was precipitated in *n*-hexane and dried in a vacuum oven at room temperature to afford the monofunctional macro-RAFT agent of *m*$PEG_{113}$-TTC (10.4 g, 97% yield) or the bifunctional macro-RAFT agent of TTC-$PEG_{136}$-TTC (6.4 g, 96% yield).

### 2.3 Dispersion polymerization of styrene mediated with the monofunctional or bifunctional macro-RAFT agent

The macro-RAFT agent of *m*$PEG_{113}$-TTC or TTC-$PEG_{136}$-TTC mediated dispersion polymerization of styrene was carried out in the methanol/water mixture (80:20 w/w) at 70 °C with the weight ratio of the styrene monomer to the solvent at 15%, in which the molar ratio of $[St]_o$:$[mPEG_{113}\text{-}TTC]_o$:$[AIBN]_o$ = 900:3:1 or $[St]_o$:$[TTC\text{-}PEG_{136}\text{-}TTC]_o$:$[AIBN]_o$ = 900:3:2. Note: the molar ratio of $[monomer]_o/[macro\text{-}RAFT]_o/[initiator]_o$ in the bifunctional macro-RAFT agent mediated dispersion polymerization is different from that in the case of the monofunctional macro-RAFT agent due to the double RAFT terminals in TTC-$PEG_{136}$-TTC, and this selection can afford the similar molecular weight of the synthesized AB and ABA block copolymers at similar monomer conversion. The polymerization procedures in the two cases of the poly(ethylene glycol) based macro-RAFT agent mediated dispersion polymerization are very similar to each other, and herein the *m*$PEG_{113}$-TTC mediated dispersion polymerization is typically introduced. Into a 25 mL Schlenk flask with a magnetic bar, *m*$PEG_{113}$-TTC (0.170 g, 0.0321 mmol), St (1.00 g, 9.60 mmol), and AIBN (1.76 mg, 0.0107 mmol) dissolved in the methanol/water mixture (80:20 w/w, 6.69 g) were added, and then the mixture was degassed with nitrogen at 0 °C for 30 min. The polymerization was started by immersing the flask into preheated oil bath at 70 °C. After a given time, the polymerization was quenched by immersing the flask in iced water and the polymerization solution was exposed to air. The monomer conversion was detected by UV-vis analysis as discussed elsewhere,[50,54] in which a given volume of the colloidal dispersion (*ca.* 1.0 mL) was filtrated twice with a 0.22 μm nylon filter, and then the filtrate was diluted with ethanol and analyzed at 245 nm. To detect the morphology of the resultant colloids, a small drop of the colloidal dispersion was deposited onto a piece of copper grid, dried under vacuum at room temperature, and then observed by transmission electron microscopy (TEM). To collect

the polymer for the GPC and $^1$H NMR analysis, the colloidal dispersion was precipitated into the mixture of diethyl ether and *n*-hexane (3:1 w/w), collected by three precipitation/filtration cycles, and then dried under vacuum at room temperature to afford the pale yellow block copolymer.

### 2.4 Apparatus and characterization

The $^1$H NMR analysis was performed on a Bruker Avance III 400MHz NMR spectrometer using $CDCl_3$ as solvent. The molecular weight and its distribution [or the polydispersity index (PDI, PDI = $M_w/M_n$)] of the synthesized block copolymers were determined by gel permeation chromatography (GPC) equipped with a Waters 600E GPC system equipped with the TSK-GEL columns and a Waters 2414 refractive index detector, where THF was used as eluent at the flow rate of 0.6 mL/min at 30.0 $^o$C and the narrow-polydispersity polystyrene was used as calibration standard. Transmission electron microscopy (TEM) observation was performed by using a Tecnai G$^2$ F20 electron microscope at an acceleration of 200 kV or a JEOL 100CX-II electron microscope at 100 kV. Differential Scanning Calorimetric (DSC) analysis was carried out on a NETZSCH DSC 204 differential scanning calorimeter under nitrogen atmosphere, in which the samples were heated to 150 $^o$C at the heating rate of 10 $^o$C/min, cooled to -80 $^o$C in 10 min, and then heated to 180 $^o$C at the heating rate of 10 $^o$C/min.

## 3 Results and discussion

### 3.1 Synthesis of *m*PEG$_{113}$-TTC and TTC-PEG$_{136}$-TTC

The poly(ethylene glycol) based macro-RAFT agents of *m*PEG$_{113}$-TTC and TTC-PEG$_{136}$-TTC were prepared by esterification reaction of the hydroxy terminal in the monohydroxyl-terminated poly(ethylene glycol) or in the dihydroxyl-terminated poly(ethylene glycol) with the carboxyl group in the trithiocarbonate of DDMAT as shown in Scheme 2 as described elsewhere.[21] Following this method, DDMAT was first reacted with $(COCl)_2$ to afford the acyl chloride modified DDMAT, and then the esterification reaction between the acyl chloride modified DDMAT and the hydroxyl-terminated poly(ethylene glycol) at 25 $^o$C was performed. To ensure complete esterification of the hydroxyl-terminated poly(ethylene glycol), 2-fold excess of the acyl chloride modified DDMAT was used. After esterification, the excess acyl chloride modified DDMAT was removed by depositing the macro-RAFT agent of *m*PEG$_{113}$-TTC or TTC-PEG$_{136}$-TTC in *n*-hexane, in which the acyl chloride modified DDMAT is soluble and the poly(ethylene glycol) based macro-RAFT agent is insoluble. Following these procedures, high yield of *m*PEG$_{113}$-TTC (97% yield) and TTC-PEG$_{136}$-TTC (96% yield) were obtained.

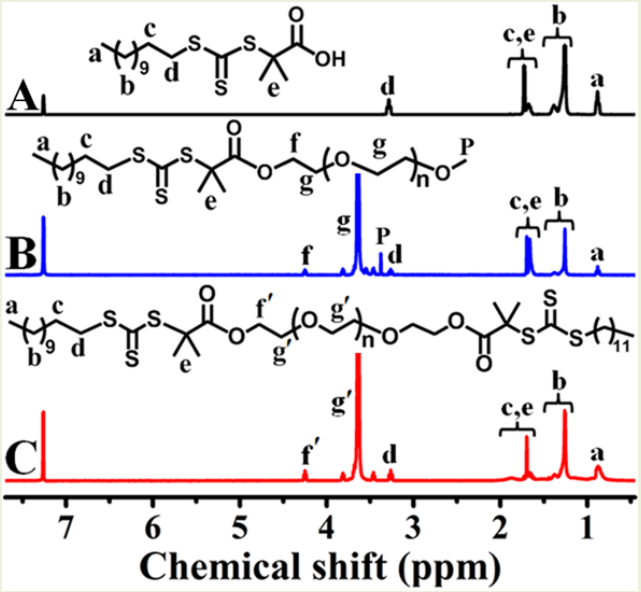


**Figure 1.** $^1$H NMR spectra of DDMAT (A), *m*PEG$_{113}$-TTC (B), and TTC-PEG$_{136}$-TTC (C) in $CDCl_3$.

Figure 1 shows the $^1$H NMR spectra of the synthesized monofunctional macro-RAFT agent of *m*PEG$_{113}$-TTC and the bifunctional macro-RAFT agent of TTC-PEG$_{136}$-TTC as well as the precursor of DDMAT. Compared to the DDMAT precursor (Figure 1A), there appear some new peaks at δ = 4.25 ppm (f or f′) corresponding to the proton of -C***H***$_2$-O(C=O) and at δ = 3.64 ppm (g or g′) corresponding to the methylene proton in the poly(ethylene glycol) chains, confirming formation of the macro-RAFT agents of *m*PEG$_{113}$-TTC (Figure 1B) and TTC-PEG$_{136}$-TTC (Figure 1C). The esterification efficiency of the hydroxyl-terminated poly(ethylene glycol) can be estimated by the area ratio of the signal at δ = 4.25 ppm (f or f′) and the signal at δ = 3.26 ppm (d) corresponding to the proton of $CH_3$-$(CH_2)_{10}$-C***H***$_2$S, and it is suggested that more than 99% *m*PEG$_{113}$-OH is converted into *m*PEG$_{113}$-TTC and 95% HO-PEG$_{136}$-OH is converted into TTC-PEG$_{136}$-TTC, respectively. The molecular weight $M_{n,NMR}$ of the monofunctional macro-RAFT agent of *m*PEG$_{113}$-TTC at 5.5 kg/mol and the bifunctional macro-RAFT agent of TTC-PEG$_{136}$-TTC at 6.8 kg/mol can be calculated by comparing the integration areas of the signal at δ = 1.10-1.45 ppm (b) and the signal at δ = 3.64 ppm (g or g′). It is found that the molecular weight $M_{n,NMR}$ of the poly(ethylene glycol) based macro-RAFT agent is slightly higher than or very close to that of the corresponding hydroxyl-terminated poly(ethylene glycol).

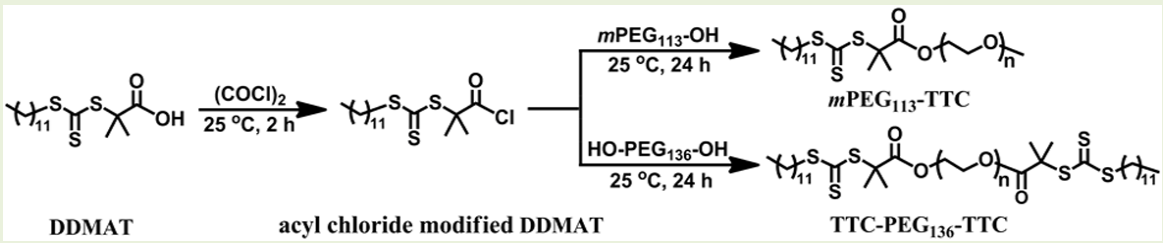


**Scheme 2.** Synthesis of *m*PEG113-TTC and TTC-PEG$_{136}$-TTC.

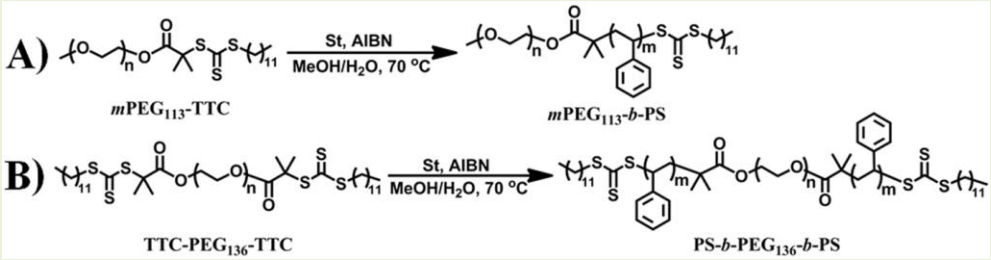


**Scheme 3.** The dispersion RAFT polymerization of styrene in the presence of *m*PEG$_{113}$-TTC (A) or TTC-PEG$_{136}$-TTC (B).

Figure 2 shows the GPC traces of the synthesized monofunctional macro-RAFT agent of *m*PEG$_{113}$-TTC and the bifunctional macro-RAFT agent of TTC-PEG$_{136}$-TTC. Based on the GPC traces, the number-average molecular weight $M_{n,GPC}$ at 9.0 kg/mol and PDI at 1.03 for the monofunctional *m*PEG$_{113}$-TTC macro-RAFT agent and $M_{n,GPC}$ at 11.5 kg/mol and PDI at 1.02 for the bifunctional TTC-PEG$_{136}$-TTC macro-RAFT agent are obtained. The $M_{n,GPC}$ of the poly(ethylene glycol) based macro-RAFT agent by GPC analysis is much higher than the corresponding $M_{n,NMR}$ by $^1$H NMR analysis, and the reason is possibly due to the polystyrene standard used in the GPC analysis.

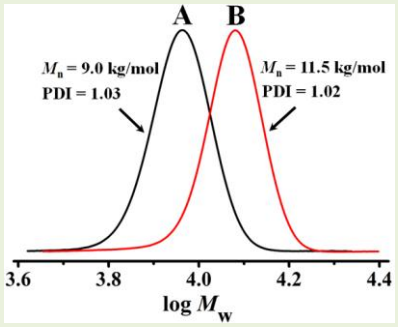


**Figure 2.** The GPC traces of *m*PEG$_{113}$-TTC (A) and TTC-PEG$_{136}$-TTC (B).

### 3.2 The monofunctional or bifunctional macro-RAFT agent mediated dispersion polymerization

To make comparison, the two dispersion RAFT polymerizations mediated with the monofunctional *m*PEG$_{113}$-TTC macro-RAFT agent and with the bifunctional TTC-PEG$_{136}$-TTC macro-RAFT agent as shown in Scheme 3 are performed under very similar conditions such as the same weight ratio of the feeding monomer to the solvent of the methanol/water mixture (80:20 w/w) at 15% and the same polymerization temperature of 70 °C. The solvent mixture of methanol/water (80:20 w/w) is chosen because it is a good solvent of the styrene monomer and the *m*PEG$_{113}$-TTC (or TTC-PEG$_{136}$-TTC) macro-RAFT agent, but a non-solvent of the PS block, which is essential for the *in situ* synthesis of the block copolymer nano-objects under the PISA condition. However, due to the double RAFT terminals in the bifunctional macro-RAFT agent, the molar ratio of [St]$_o$:[macro-RAFT agent]$_o$:[AIBN]$_o$, 900:3:2 in the case of the TTC-PEG$_{136}$-TTC macro-RAFT agent mediated dispersion polymerization and 900:3:1 in the case of the *m*PEG$_{113}$-TTC macro-RAFT agent mediated dispersion polymerization, is slightly different. This difference ensures these two dispersion RAFT polymerizations with similar polymerization kinetics and the similar molecular weight of the synthesized AB diblock copolymer and the BAB triblock copolymer at a given monomer conversion as discussed subsequently.

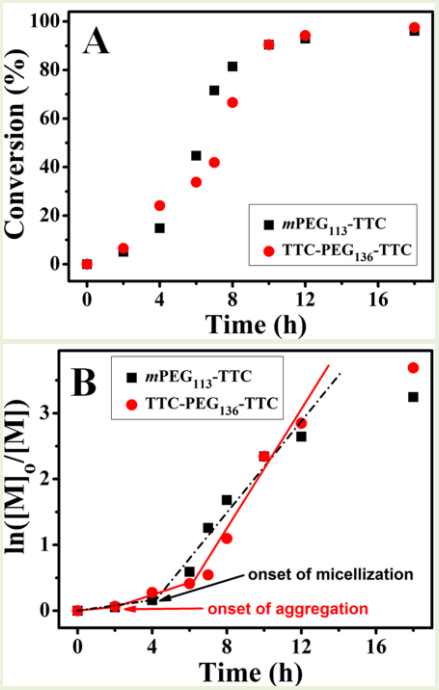


**Figure 3.** The monomer conversion-time plots (A) and the ln([M]o/[M])-time plots (B) for the dispersion RAFT polymerization of styrene in the presence of *m*PEG$_{113}$-TTC or TTC-PEG$_{136}$-TTC.

In the general monofunctional macro-RAFT agent mediated dispersion polymerization especially in the case of inactive monomers such as styrene, an initial homogeneous polymerization and a subsequent heterogeneous polymerization are usually observed even by the naked eye.[38,39,44-48] The initial homogeneous stage is due to the synthesized block copolymer containing a relatively short solvophobic block and therefore being soluble in the polymerization medium at the polymerization temperature. With the proceeding of the RAFT polymerization, the solvophobic block extends and the block copolymer becomes molecularly insoluble, and self-assembly of the synthesized block copolymer occurs, and then the subsequent heterogeneous polymerization takes place under dispersion condition. In the present monofunctional *m*PEG$_{113}$-TTC macro-RAFT agent mediated dispersion polymerization, the similar polymerization kinetics including an initial 4 h homogeneous stage below 14.8% monomer conversion and a subsequent heterogeneous stage is observed as shown in Figure 3A. Figure 3B shows the ln([M]$_0$/[M]) *vs* polymerization time plot, in which a two-stage plot containing a gradient linear stage corresponding to the initial

homogeneous polymerization and a steep linear one corresponding to the later heterogeneous polymerization is observed. This suggests that the present monofunctional *m*PEG$_{113}$-TTC macro-RAFT agent mediated dispersion polymerization runs similarly with those discussed elsewhere.[38,39,44-48] The *in situ* synthesized diblock copolymer nano-objects of *m*PEG$_{113}$-*b*-PS can be uniformly dispersed in the polymerization medium even at the high monomer conversion of 96.1% in 18 h (Figure 4). The dispersion polymerization in the presence of the bifunctional TTC-PEG$_{136}$-TTC macro-RAFT agent undergoes a similar polymerization kinetics as shown in Figure 3. However, two differences have been observed in the bifunctional TTC-PEG$_{136}$-TTC macro-RAFT agent mediated dispersion polymerization. First, a shorter homogeneous stage exists in the bifunctional TTC-PEG$_{136}$-TTC macro-RAFT agent mediated dispersion polymerization than that in the case of the monofunctional *m*PEG$_{113}$-TTC macro-RAFT agent as indicated by the insets in Figure 3B (2 h *vs* 4 h). Second, the *in situ* synthesized PS-*b*-PEG$_{136}$-*b*-PS triblock copolymer cannot be uniformly dispersed in the polymerization medium. Note: to discern the synthesized block polymer distributed in the polymerization medium, all samples are transferred from the Schlenk flasks into glass bottles without any dilution. As shown in Figure 4, gel-like polymer deposits on the bottom of the bottles even at low monomer conversion of 6.51% in 2 h. At high monomer conversion of 97.5% in 18 h, some powder-like polymer attached on the wall of the bottles and deposited on the bottom of the bottles is discerned. The different appearance of the gel-like polymer in the initial polymerization stage and the powder-like polymer in the later polymerization stage is partly due to the different glass transition temperatures ($T_g$s) of the synthesized PS-*b*-PEG$_{136}$-*b*-PS triblock copolymers with different DP of the PS block, which will be discussed subsequently.

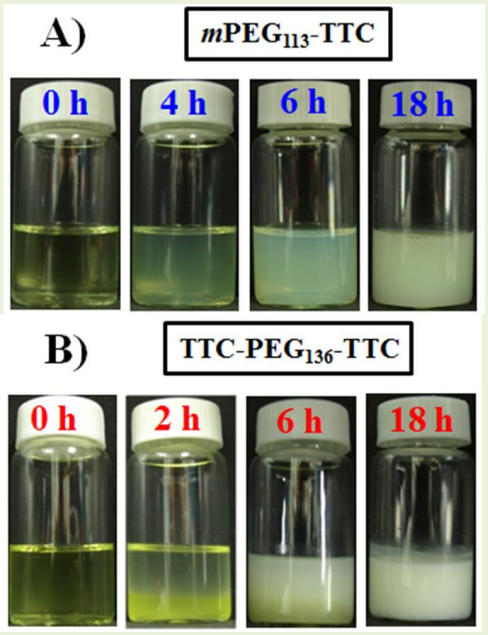


**Figure 4.** Optical photos of the polymerization solution of the dispersion RAFT polymerization in the presence of the monofunctional *m*PEG$_{113}$-TTC macro-RAFT agent (A) or the bifunctional TTC-PEG$_{136}$-TTC macro-RAFT agent (B) at different polymerization times.

The synthesized block copolymers, the *m*PEG$_{113}$-*b*-PS diblock copolymer in the case of the monofunctional *m*PEG$_{113}$-TTC macro-RAFT agent mediated dispersion polymerization and the PS-*b*-PEG$_{136}$-*b*-PS triblock copolymer in the case of the bifunctional TTC-PEG$_{136}$-TTC macro-RAFT agent mediated dispersion polymerization, are separated and then characterized by $^1$H NMR analysis (Figure S1) and GPC analysis (Figure 5). As shown in Figure S1, the *m*PEG$_{113}$-*b*-PS diblock copolymers and the PS-*b*-PEG$_{136}$-*b*-PS triblock copolymers have very similar $^1$H NMR spectra. With increase in polymerization time, the proton resonance signals at $\delta$ = 6.26-7.23 ppm (j, l, k or j′, l′, k′) corresponding to the PS block increase gradually, indicating the chain extension of the PS block in the *m*PEG$_{113}$-*b*-PS diblock copolymers and in the PS-*b*-PEG$_{136}$-*b*-PS triblock copolymers. By comparing the proton resonance signals at $\delta$ = 6.26-7.23 ppm (j, l, k or j′, l′, k′) and $\delta$ = 3.64 ppm (g or g′), the molecular weight $M_{n,NMR}$ of the *m*PEG$_{113}$-*b*-PS diblock copolymer and the PS-*b*-PEG$_{136}$-*b*-PS triblock copolymer synthesized at different polymerization times is calculated and summarized in Figure 5. From Figure 5, the different GPC traces for the *m*PEG$_{113}$-*b*-PS diblock copolymer and the PS-*b*-PEG$_{136}$-*b*-PS triblock copolymer are clearly discerned. That is, the *m*PEG$_{113}$-*b*-PS diblock copolymer shows monomodal GPC traces or GPC traces with very slight shoulder at the high molecular weight side at high monomer conversion; whereas all the GPC traces of the PS-*b*-PEG$_{136}$-*b*-PS triblock copolymer have an obvious shoulder at high molecular weight side even at low monomer conversion of 6.51% in 2 h. Correspondingly, the PDI of the *m*PEG$_{113}$-*b*-PS diblock copolymer is generally below 1.1, and the PDI of the PS-*b*-PEG$_{136}$-*b*-PS triblock copolymer locates 1.2 at moderate monomer conversion and it further increases to 1.35 at high monomer conversion. This suggests that the dispersion RAFT polymerization mediated with the bifunctional TTC-PEG$_{136}$-TTC macro-RAFT agent is not as well controlled as that mediated with the monofunctional *m*PEG$_{113}$-TTC macro-RAFT agent. The relatively high PDI of the PS-*b*-PEG$_{136}$-*b*-PS triblock copolymer is possibly due to the triblock copolymer being not uniformly distributed in the polymerization medium as discussed above, which makes different accessibility of the styrene monomer to the triblock copolymer nucleus and therefore results in the relatively broad distribution of the polymer molecular weight. Despite the relatively high PDI of the PS-*b*-PEG$_{136}$-*b*-PS triblock copolymer, the linear increase in the polymer molecular weight whether by GPC analysis ($M_{n,GPC}$) or by $^1$H NMR analysis ($M_{n,NMR}$) with monomer conversion is detected (Figure 5), which is similar to that in the monofunctional *m*PEG$_{113}$-TTC macro-RAFT agent mediated dispersion polymerization. It is found that $M_{n,GPC}$ of the synthesized *m*PEG$_{113}$-*b*-PS diblock copolymer or the PS-*b*-PEG$_{136}$-*b*-PS triblock copolymer by GPC analysis is slightly higher than the corresponding $M_{n,NMR}$ by $^1$H NMR analysis, which is very close to the theoretical molecular weight $M_{n,th}$ by the monomer conversion according to eqn 1 as described elsewhere,[55] and the reason is possibly due to the polystyrene standard employed in the GPC analysis.

$$M_{n,th} = \frac{[\text{monomer}]_0 \times M_{\text{monomer}}}{[\text{RAFT}]_0} \times conversion + M_{\text{RAFT}} \quad (1)$$

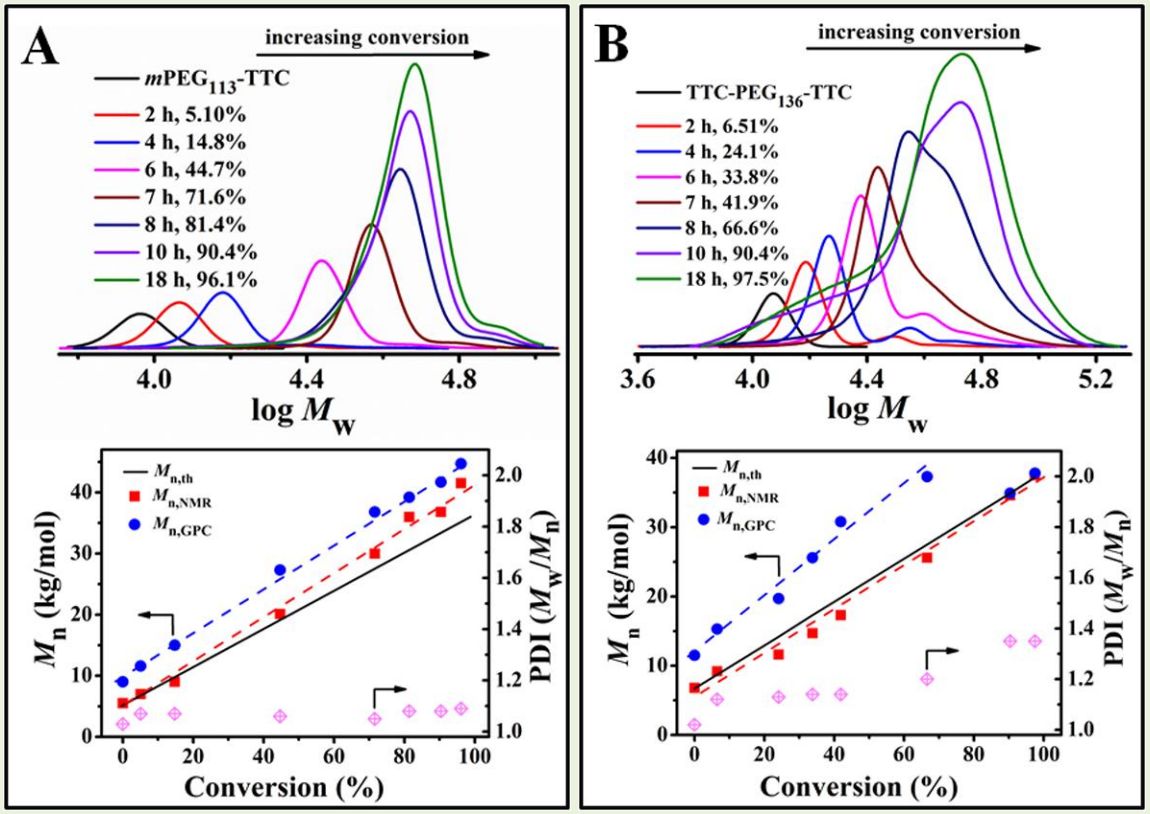


**Figure 5.** The GPC traces and the evolution of the molecular weight and the PDI ($M_w/M_n$) values of the *m*PEG$_{113}$-*b*-PS diblock copolymers (A) and the PS-*b*-PEG$_{136}$-*b*-PS triblock copolymers (B) synthesized through the dispersion RAFT polymerization mediated with the monofunctional macro-RAFT agent of *m*PEG$_{113}$-TTC and with the bifunctional macro-RAFT agent of TTC-PEG$_{136}$-TTC.

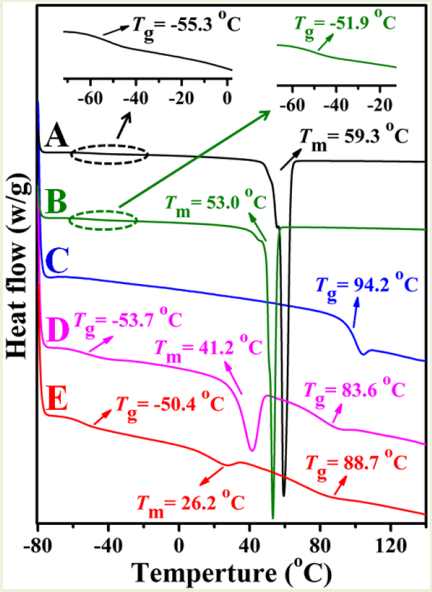


**Figure 6**. The DSC thermograms of *m*PEG$_{113}$-TTC (A), TTC-PEG$_{136}$-TTC (B), PS$_{192}$-TTC (C), *m*PEG$_{113}$-*b*-PS$_{288}$ (D) and PS$_{146}$-*b*-PEG$_{136}$-*b*-PS$_{146}$ (E).

The typical diblock copolymer of *m*PEG$_{113}$-*b*-PS$_{288}$ and the triblock copolymer of PS$_{146}$-*b*-PEG$_{136}$-*b*-PS$_{146}$ as well as the reference polymers of *m*PEG$_{113}$-TTC, TTC-PEG$_{136}$-TTC and PS$_{192}$-TTC (seeing the synthesis in ref. 50) are further characterized by DSC analysis. From the DSC thermograms shown in Figure 6, two conclusions are made. First, the PEG block and the PS block either in the *m*PEG$_{113}$-*b*-PS$_{288}$ diblock copolymer or in the PS$_{146}$-*b*-PEG$_{136}$-*b*-PS$_{146}$ triblock copolymer are immiscible,[56] since two separate $T_g$s corresponding to the PEG block and the PS block are detected (Figures 6D and 6E). Second, it seems that the PEG block in the *m*PEG$_{113}$-*b*-PS$_{288}$ diblock copolymer is more crystalline than that in the PS$_{146}$-*b*-PEG$_{136}$-*b*-PS$_{146}$ triblock copolymer,[57] since a sharp and narrow melting temperature ($T_m$) is detected in the former case (Figure 6D). The reason that the PEG block in the *m*PEG$_{113}$-*b*-PS$_{288}$ diblock copolymer is more crystalline than that in the PS$_{146}$-*b*-PEG$_{136}$-*b*-PS$_{146}$ triblock copolymer needs further study.

As discussed previously,[27,33-50] the general macro-RAFT agent mediated dispersion polymerization affords the *in situ* synthesis of block copolymer nano-objects, and the size or morphology of the block copolymer nano-objects changes with the extension of the solvophobic block during the dispersion RAFT polymerization. The morphologies of the *m*PEG$_{113}$-*b*-PS diblock copolymers and the PS-*b*-PEG$_{136}$-*b*-PS triblock copolymers prepared at different monomer conversions are checked and the results are shown in Figures 7-9. The TEM images shown in Figure 7 clearly suggest formation of the *m*PEG$_{113}$-*b*-PS diblock copolymer nanoparticles in the monofunctional *m*PEG$_{113}$-TTC macro-RAFT agent mediated dispersion polymerization. These nanoparticles are expected to have a corona-core structure, in which the solvophilic PEG block forms the corona and the solvophobic PS block forms the core. The average diameter ($D$) of the *m*PEG$_{113}$-*b*-PS nanoparticles is evaluated by statistical analysis of above 100 particles, and it

increases from 11 to 25 nm with the increasing polymerization time from 4 to 18 h or with the extending DP of the PS block from 44 to 288 as shown in Figure 8. Figure 9 shows the TEM images of the PS-*b*-$PEG_{136}$-*b*-PS triblock copolymers synthesized through the bifunctional TTC-$PEG_{136}$-TTC macro-RAFT agent mediated dispersion polymerization at different polymerization time, in which the mixture of small-sized nanoparticles and large-sized aggregates is observed even at low monomer conversion of 6.51%. Interestingly, some of the small-sized nanoparticles are attached on the large-sized aggregates, which is believed to increase the dispersion of the large-sized aggregates in the solvent during the dispersion RAFT polymerization. The large-sized aggregates should be due to the bridge connection between the two terminal solvophobic PS blocks in the PS-*b*-$PEG_{136}$-*b*-PS triblock copolymer, which leads to formation of the large-sized gel-like networks of BAB triblock copolymer. The small-sized triblock copolymer nanoparticles are expected to have a flower-like corona-core structure, in which the solvophilic central PEG block forms the loop corona and the two terminal solvophobic PS blocks form the core as shown in Scheme 1A. The size of the small-sized triblock copolymer nanoparticles is not precisely calculated, since it is not easy to identify the single nanoparticles from the mixture of the small-sized nanoparticles and the large-sized aggregates. However, by comparing the TEM images shown in Figure 7 and Figure 9, it seems that the smallest PS-*b*-$PEG_{136}$-*b*-PS triblock copolymer nanoparticles is even larger than the *m*$PEG_{113}$-*b*-PS diblock copolymer nanoparticles with the similar polymer composition. For example, the size of the smallest $PS_{146}$-*b*-$PEG_{136}$-*b*-$PS_{146}$ triblock copolymer nanoparticles is above 40 nm (Figure 9D), which is much larger than 25 nm of the *m*$PEG_{113}$-*b*-$PS_{288}$ diblock copolymer nanoparticles shown in Figure 7D, although the $PS_{146}$-*b*-$PEG_{136}$-*b*-$PS_{146}$ triblock copolymer has a similar composition to the *m*$PEG_{113}$-*b*-$PS_{288}$ diblock copolymer.

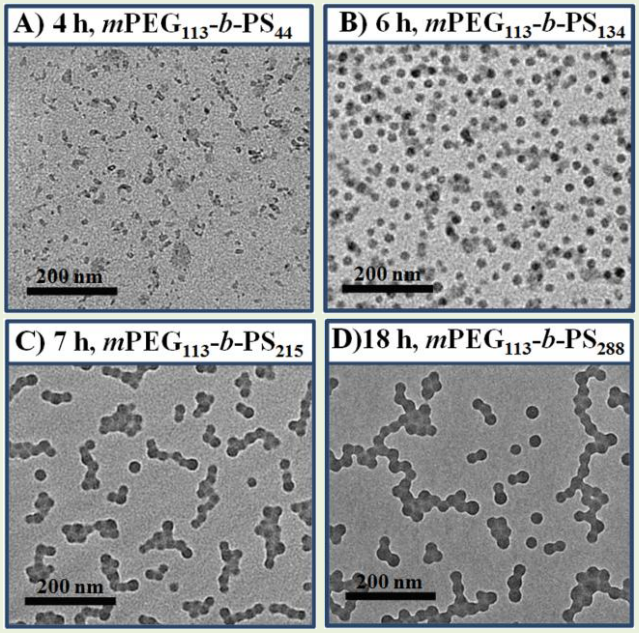


**Figure 7.** TEM images of the *m*$PEG_{113}$-*b*-PS diblock copolymer nanoparticles prepared through the monofunctional *m*$PEG_{113}$-TTC macro-RAFT agent mediated dispersion polymerization at the polymerization time of 4 h (A), 6 h (B), 7 h (C) and 18 h (D).

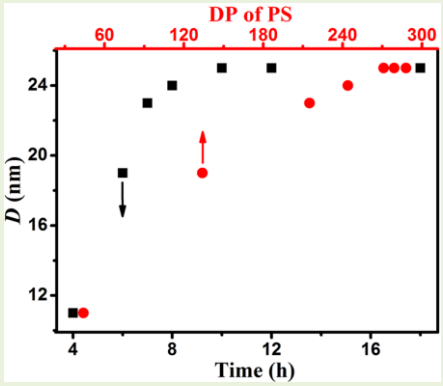


**Figure 8.** The evolution of the average diameter (*D*) of the *m*$PEG_{113}$-*b*-PS diblock copolymer nanoparticles with the polymerization time or the DP of PS block.

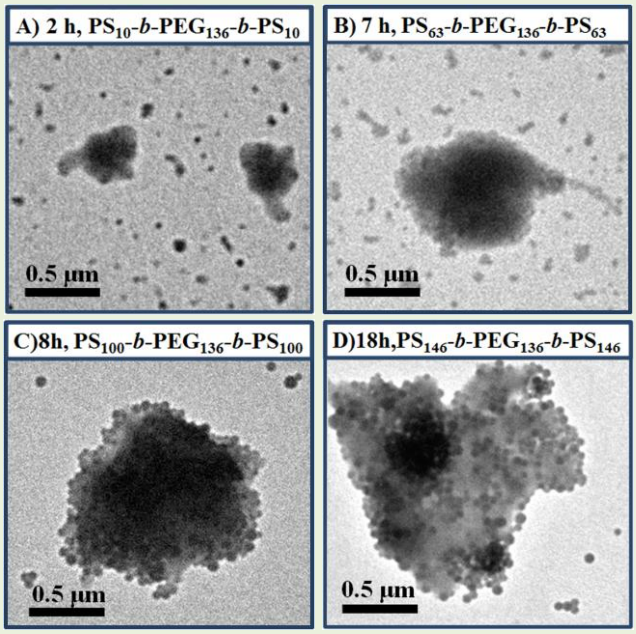


**Figure 9.** TEM images of the PS-*b*-$PEG_{136}$-*b*-PS triblock copolymers prepared through the bifunctional TTC-$PEG_{136}$-TTC macro-RAFT agent mediated dispersion polymerization at the polymerization time of 2 h (A), 7 h (B), 8 h (C) and 18 h (D).

As discussed previously,[40,44,47] the chain length of the macro-RAFT agent exerts great influence on the polymerization kinetics and on the morphology of block copolymer. Generally, a long macro-RAFT agent leads to formation of block copolymer nanoparticles (nanospheres) and a short macro-RAFT agent leads to formation of worms or vesicles. To make further comparison, two short macro-RAFT agents, the monofunctional *m*$PEG_{45}$-TTC macro-RAFT agent and the bifunctional TTC-$PEG_{45}$-TTC macro-RAFT agent, were synthesized and their mediated dispersion polymerizations were checked. Similarly, the monofunctional *m*$PEG_{45}$-TTC macro-RAFT agent mediated dispersion polymerization leas to colloids of the *m*$PEG_{45}$-*b*-PS diblock copolymer and the bifunctional TTC-$PEG_{45}$-TTC macro-RAFT agent mediated dispersion polymerization leads to gel-like polymer of the PS-*b*-$PEG_{45}$-*b*-PS triblock copolymer (Figure S2). In the cases of the short bifunctional TTC-$PEG_{45}$-TTC macro-RAFT agent mediated dispersion polymerization, serious phase

separation (Figure S2) and therefore slow polymerization kinetics (Figure S3) were observed. The reason is due to the solvophilic $PEG_{45}$ block in the PS-*b*-$PEG_{45}$-*b*-PS triblock copolymer being too short to keep the triblock copolymer suspending in the polymerization medium. Similarly, bimodal GPC traces of the synthesized PS-*b*-$PEG_{45}$-*b*-PS triblock copolymer were found (Figure S4 and Table S1). In the cases of the short monofunctional *m*$PEG_{45}$-TTC macro-RAFT agent mediated dispersion polymerization, the dispersion RAFT polymerization ran smoothly, good control in both the molecular weight of the *m*$PEG_{45}$-*b*-PS diblock copolymer and the molecular weight distribution were achieved (Figures S5 and S6). Different from the nanoparticles synthesized in the case of the long monofunctional *m*$PEG_{113}$-TTC macro-RAFT agent mediated dispersion polymerization, vesicles were formed in the short monofunctional *m*$PEG_{45}$-TTC macro-RAFT agent mediated dispersion polymerization just as expected (Figure S7).

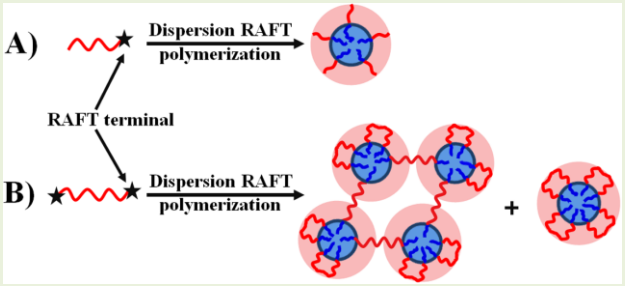


**Scheme 4.** Schematic dispersion RAFT polymerization mediated with the monofunctional macro-RAFT agent (A) or the bifunctional macro-RAFT agent (B).

Summarily, our main findings are summarized in Scheme 4. That is, the monofunctional *m*$PEG_{113}$-TTC macro-RAFT agent mediated dispersion polymerization of styrene affords the *in situ* synthesis of the colloidal nanoparticles of the *m*$PEG_{113}$-*b*-PS diblock copolymer, and the bifunctional TTC-$PEG_{136}$-TTC macro-RAFT agent mediated dispersion polymerization leads to the mixture of the flower-like corona-core nanoparticles and gel-like networks of the PS-*b*-$PEG_{136}$-*b*-PS triblock copolymer.

## 4 Conclusions

Through esterification reaction between the monohydroxyl-terminated or dihydroxyl-terminated poly(ethylene glycol) and the trithiocarbonate of DDMAT, the monofunctional macro-RAFT agent of *m*$PEG_{113}$-TTC and the bifunctional macro-RAFT agent of TTC-$PEG_{136}$-TTC are prepared. The two cases of dispersion RAFT polymerizations of styrene in the methanol/water mixture mediated with the monofunctional *m*$PEG_{113}$-TTC macro-RAFT agent and with the bifunctional TTC-$PEG_{136}$-TTC macro-RAFT agent are compared. It is found that these two dispersion RAFT polymerizations under similar condition have similar polymerization rate, and almost full monomer conversion is achieved in 18 h. The molecular weight of the *m*$PEG_{113}$-*b*-PS diblock copolymer synthesized *via* the *m*$PEG_{113}$-TTC mediated dispersion RAFT polymerization and the molecular weight of the PS-*b*-$PEG_{136}$-*b*-PS triblock copolymer synthesized *via* the TTC-$PEG_{136}$-TTC mediated dispersion RAFT polymerization linearly increase with the monomer conversion, whereas the control over the PDI of the PS-*b*-$PEG_{136}$-*b*-PS triblock copolymer is not as good as that of the *m*$PEG_{113}$-*b*-PS diblock copolymer. The monofunctional *m*$PEG_{113}$-TTC macro-RAFT agent mediated dispersion polymerization affords the *in situ* synthesis of the *m*$PEG_{113}$-*b*-PS diblock copolymer nanoparticles, which can be uniformly distributed in the polymerization medium and whose size increases from 11 to 25 nm with extending DP of the PS block from 44 to 288. Whereas, the bifunctional TTC-$PEG_{136}$-TTC macro-RAFT agent mediated dispersion polymerization leads to the mixture of flower-like corona-core nanoparticles and gel-like networks of the PS-*b*-$PEG_{136}$-*b*-PS triblock copolymer, which tends to deposit from the polymerization medium and is deemed to contribute the relatively high PDI of the PS-*b*-$PEG_{136}$-*b*-PS triblock copolymer.

## Acknowledgments

The financial support by National Science Foundation of China (№ 21274066) and PCSIRT (IRT1257) is gratefully acknowledged.

## Notes and references

[a] *Key Laboratory of Functional Polymer Materials of the Ministry of Education, Collaborative Innovation Center of Chemical Science and Engineering (Tianjin), Institute of Polymer Chemistry, Nankai University, Tianjin 300071, China.* [b] *Department of Chemistry, Tianjin University, Tianjin 300072, China.*
**To whom correspondence should be addressed. E-mail: wqzhang@nankai.edu.cn, Tel: 86-22-23509794, Fax: 86-22-23503510.*

† Electronic Supplementary Information (ESI) available: Scheme S1 showing the chemical structure of DDMAT, Figure S1 showing the $^1$H NMR spectra of the *m*$PEG_{113}$-*b*-PS diblock copolymer the PS-*b*-$PEG_{136}$-*b*-PS triblock copolymer, Figures S3-S7 and Tables summarizing the dispersion polymerization mediated by the short macro-RAFT agents of the monofunctional *m*$PEG_{45}$-TTC and the bifunctional TTC-$PEG_{45}$-TTC. See DOI: 10.1039/b000000x/

1 G. Riess, *Prog. Polym. Sci.*, 2003, **28**, 1107-1170.
2 M. J. Monteiro and M. F. Cunningham, *Macromolecules*, 2012, 45, 4939-4957.
3 B. Charleux, G. Delaittre, J. Rieger and F. D'Agosto, *Macromolecules*, 2012, **45**, 6753-6765.
4 J.-T. Sun, C.-Y. Hong, and C.-Y. Pan, *Polym. Chem.*, 2013, **4**, 873-881.
5 T. Azzam and A. Eisenberg, *Angew. Chem., Int. Ed.*, 2006, **45**, 7443-7447
6 C. Pietsch, U. Mansfeld, C. Guerrero-Sanchez, S. Hoeppener, A. Vollrath, M. Wagner, R. Hoogenboom, S. Saubern, S. H. Thang, C. R. Becer, J. Chiefari and U. S. Schubert, *Macromolecules*, 2012, **45**, 9292-9302.
7 H.-N. Lee, Z. Bai, N. Newell and T. P. Lodge, *Macromolecules*, 2010, **43**, 9522-9528.
8 O. Colombani, M. Ruppel, M. Burkhardt, M. Drechsler, M. Schumacher, M. Gradzielski, R. Schweins and A. H. E. Müller, *Macromolecules*, 2007, **40**, 4351-4362.
9 R. T. Pearson, N. J. Warren, A. L. Lewis, S. P. Armes and G. Battaglia, *Macromolecules*, 2013, **46**, 1400-1407.
10 Y. Hu, V. Darcos, S. Monge and S. Li, J. *Polym. Sci., Part A: Polym. Chem.*, 2013, **51**, 3274-3283.
11 X.-Z. Yang, Y.-C. Wang, L.-Y. Tang, H. Xia, and J. Wang, *J. Polym. Sci., Part A: Polym. Chem.*, 2008, **46**, 6425-6434.
12 M. Dan, Y. Su, X. Xiao, S. Li, and W. Zhang, *Macromolecules* 2013, **46**, 3137-3146.
13 A. J. de Graaf, K. W. M. Boere, J. Kemmink, R. G. Fokkink, C. F. van Nostrum, D. T. S. Rijkers, J. van der Gucht, H. Wienk, M.

Baldus, E. Mastrobattista, T. Vermonden and W. E. Hennink, *Langmuir*, 2011, **27**, 9843-9848.
14 K. Skrabania, W. Li and A. Laschewsky, *Macromol. Chem. Phys.*, 2008, **209**, 1389-1403.
15 S. Li, Y. Su, M. Dan and W. Zhang, *Polym. Chem.*, 2014, **5**, 1219-1228.
16 F. F. Taktak and V. Bütün, *Polymer*, 2010, **51**, 3618-3626.
17 F. C. Giacomelli, I. C. Riegel, C. L. Petzhold, N. P. da Silveira and P. Štěpánek, *Langmuir*, 2009, **25**, 731-738.
18 C. Charbonneau, M. D. S. Lima, C. Chassenieux, O. Colombani and T. Nicolai, *Phys. Chem. Chem. Phys.*, 2013, **15**, 3955-3964.
19 M. A. Ward, T. K. Georgiou, *J. Polym. Sci., Part A: Polym. Chem.*, 2013, **51**, 2850-2859.
20 Y. Zhou, N. Sharma, P. Deshmukh, R. K. Lakhman, M. Jain, and R. M. Kasi, *J. Am. Chem. Soc.*, 2012, **134**, 1630-1641.
21 Y. He and T. P. Lodge, *Macromolecules*, 2008, **41**, 167-174.
22 T. G. O'Lenick, N. Jin, J. W. Woodcock and B. Zhao, *J. Phys. Chem. B*, 2011, **115**, 2870-2881.
23 S. E. Kirkland, R. M. Hensarling, S. D. McConaughy, Y. Guo, W. L. Jarrett and C. L. McCormick, *Biomacromolecules*, 2008, **9**, 481-486.
24 D. Han, O. Boissiere, S. Kumar, X. Tong, L. Tremblay and Y. Zhao, *Macromolecules*, 2012, **45**, 7440-7445.
25 Y. D. Zaroslov, G. Fytas, M. Pitsikalis, N. Hadjichristidis, O. E. Philippova and A. R. Khokhlov, *Macromol. Chem. Phys*., 2005, **206**, 173-179.
26 X. Zhang, F. Boisson, O. Colombani, C. Chassenieux and B. Charleux, *Macromolecules*, 2014, **47**, 51-60.
27 X. Zhang, J. Rieger and B. Charleux, *Polym. Chem.*, 2012, **3**, 1502-1509.
28 Z. Jia, V. A. Bobrin, N. P. Truong, M. Gillard and M. J. Monteiro, *J. Am. Chem. Soc.*, 2014, **136**, 5824-5827.
29 C. N. Urbani and M. J. Monteiro, *Macromolecules*, 2009, **42**, 3884-3886.
30 R. W. Simms, T. P. Davis and M. F. Cunningham, *Macromol. Rapid Commun*., 2005, **26**, 592-596.
31 C. J. Ferguson, R. J. Hughes, D. Nguyen, B. T. T. Pham, R. G. Gilbert, A . K. Serelis, C. H. Such, B. S. Hawkett, *Macromolecules*, 2005, **38**, 2191-2204.
32 D. E. Ganeva, E. Sprong, H. de Bruyn, G. G. Warr, C. H. Such, and B. S. Hawkett, *Macromolecules*, 2007, **40**, 6181-6189.
33 X. Zhang, S. Boissé, C. Bui, P.-A. Albouy, A. Brûlet, M.-H. Li, J. Rieger and B. Charleux, *Soft Matter*, 2012, **8**, 1130-1141.
34 J. Rieger, C. Grazon, B. Charleux, D. Alaimo and C. J. Jérôme, *J. Polym. Sci., Part A: Polym. Chem.*, 2009, **47**, 2373-2390.
35 W.-D. He, X.-L. Sun, W.-M. Wan and C.-Y. Pan, *Macromolecules*, 2011, **44**, 3358-3365.
36 W.-J. Zhang, C.-Y. Hong and C.-Y. Pan, *Macromolecules*, 2014, **47**, 1664-1671.
37 C.-Q. Huang and C.-Y. Pan, *Polymer*, 2010, **51**, 5115-5121.
38 A. Blanazs, J. Madsen, G. Battaglia, A. J. Ryan and S. P. Armes, *J. Am. Chem. Soc.*, 2011, **133**, 16581-16587.
39 N. J. Warren, O. O. Mykhaylyk, D. Mahmood, A. J. Ryan and S. P. Armes, *J. Am. Chem. Soc*., 2014, **136**, 1023-1033.
40 L. A. Fielding, M. J. Derry, V. Ladmiral, J. Rosselgong, A. M. Rodrigues, L. P. D. Ratcliffe, S. Sugihara and S. P. Armes, *Chem. Sci*., 2013, **4**, 2081-2087.
41 G. Liu, Q. Qiu and Z. An, *Polym. Chem*., 2012, **3**, 504-513.
42 G. Liu, Q. Qiu, W. Shen and Z. An, *Macromolecules*, 2011, **44**, 5237-5245.
43 W. Shen, Y. Chang, G. Liu, H. Wang, A. Cao and Z. An, *Macromolecules*, 2011, **44**, 2524-2530.
44 M. Dan, F. Huo, X. Zhang, X. Wang and W. Zhang, *J. Polym. Sci., Part A: Polym. Chem.*, 2013, **51**, 1573-1584.
45 X. Xiao, S. He, M. Dan, Y. Su, F. Huo and W. Zhang, *J. Polym. Sci., Part A: Polym. Chem.*, 2013, **51**, 3177-3190.
46 X. Wang, J. Xu, Y. Zhang and W. Zhang, *J. Polym. Sci., Part A: Polym. Chem.*, 2012, **50**, 2452-2462.
47 Y. Su, X. Xiao, S. Li, M. Dan, X. Wang and W. Zhang, *Polym. Chem.*, 2014, **5**, 578-587.
48 Q. Li, C. Gao, S. Li , F. Huo and W. Zhang, *Polym. Chem.*, 2014, **5**, 2961-2972.
49 F. Huo, C. Gao, M. Dan, X. Xiao, Y. Su and W. Zhang, *Polym. Chem.*, 2014, **5**, 2736-2746.
50 C. Gao, Q. Li, Y. Cui, F. Huo, S. Li, Y. Su and W. Zhang, *J. Polym. Sci., Part A: Polym. Chem.*, 2014, **52**, 2155-2165.
51 Y. Zhou, S. Ahn, R. K. Lakhman, M. Gopinadhan, C. O. Osuji and R. M. Kasi, *Macromolecules*, 2011, **44**, 3924-3934
52 M. Achilleos, T. M. Legge, S. Perrier and C. S. Patrickios, *J. Polym. Sci., Part A: Polym. Chem.*, 2008, **46**, 7556-7565.
53 J. T. Lai, D. Filla and R. Shea, *Macromolecules*, 2002, **35**, 6754-6756.
54 Y. Q. Wang, H. Q. Xin and W. L. Xu, *Spectrosc. Spect. Anal*., 2007, **27**, 743-746.
55 H. de Brouwer, M. A. J. Schellekens, B. Klumperman, M. J. Monteiro and A. L. German, *J. Polym. Sci., Part A: Polym. Chem.*, 2000, **38**, 3596-3603.
56 Y. Zhang, M. Pan, C. Liu and J. Huang, *J. Polym. Sci., Part A: Polym. Chem.*, 2008, **46**, 2624-2631.
57 J.-T. Xu , J.-J. Yuan and S.-Y. Cheng, *Eur. Polym. J.*, 2003, **39**, 2091-2098.